Experimental Neurology 311 (2019) 247–256

Contents lists available at ScienceDirect

Experimental Neurology

journal homepage: www.elsevier.com/locate/yexnr

Research paper

Gene expression profiling in a mouse model of Dravet syndrome

Nicole A. Hawkins, Jeffrey D. Calhoun, Alexandra M. Huffman, Jennifer A. Kearney*

Department of Pharmacology, Northwestern University Feinberg School of Medicine, Chicago, IL 60611, USA

ARTICLE INFO

Keywords:
Epilepsy
Epileptic encephalopathy
Seizure
Voltage-gated sodium channel
Gene expression
RNA-seq

ABSTRACT

Dravet syndrome is a severe, early-onset epileptic encephalopathy frequently resulting from de novo mutations of *SCN1A*. Mice with heterozygous deletion of *Scn1a* (*Scn1a*$^{+/-}$) model many features of Dravet syndrome, including spontaneous seizures and premature lethality. *Scn1a*$^{+/-}$ mice exhibit variable phenotype penetrance and expressivity dependent upon the strain background. On the 129S6/SvEvTac (129) strain, *Scn1a*$^{+/-}$ mice do not display an overt phenotype. However *Scn1a*$^{+/-}$ mice on the [129S6xB6]F1 strain (F1.*Scn1a*$^{+/-}$) exhibit juvenile-onset spontaneous seizures and premature lethality. QTL mapping identified several modifier loci responsible for strain-dependent differences in survival of *Scn1a*$^{+/-}$ mice, but these loci do not account for all the observed phenotypic variance. Global RNA-seq analysis was performed to identify additional genes and pathways that may contribute to variable phenotypes. Hippocampal gene expression was analyzed in wild-type (WT) and *Scn1a*$^{+/-}$ mice on both F1 and 129 strains, at two time points during disease development. There were few gene expression differences between 129.WT and 129.*Scn1a*$^{+/-}$ mice and approximately 100 genes with small expression differences (6–36%) between F1.WT and F1.*Scn1a*$^{+/-}$ mice. Strain-specific gene expression differences were more pronounced, with dozens of genes with > 1.5-fold expression differences between 129 and F1 strains. Age-specific and seizure-related gene expression differences were most prominent, with hundreds of genes with > 2-fold differences in expression identified between groups with and without seizures, suggesting potential differences in developmental trajectory and/or homeostatic plasticity during disease onset. Global expression differences in the context of *Scn1a* deletion may account for strain-dependent variation in seizure susceptibility and survival observed in *Scn1a*$^{+/-}$ mice.

1. Introduction

Dravet syndrome is an infant-onset epileptic encephalopathy frequently associated with a poor prognosis. Individuals with Dravet syndrome exhibit various types of seizures, as well as comorbid psychomotor and cognitive delays, and have a significant risk for sudden unexplained death in epilepsy (SUDEP) (Dravet, 2011; Dravet and Oguni, 2013). Over 80% of individuals diagnosed with Dravet syndrome have a mutation in *SCN1A,* with nearly all variants arising de novo (Claes et al., 2009). The majority of *SCN1A* mutations identified in Dravet syndrome are nonsense, frameshift, or splice site mutations that result in protein truncation, while the remaining missense mutations are believed to result in loss of protein function (Claes et al., 2009; De Jonghe, 2011; Scheffer et al., 2009). This suggests that *SCN1A* haploinsufficiency is responsible for Dravet syndrome.

Mouse models of Dravet syndrome have been generated by disruption of the *Scn1a* gene (Miller et al., 2014; Yu et al., 2006). Mice with heterozygous deletion of *Scn1a* (*Scn1a*$^{+/-}$) recapitulate many features of Dravet syndrome, including spontaneous generalized tonic-clonic seizures, seizures provoked by hyperthermia and premature lethality (Hawkins et al., 2016; Kalume et al., 2013; Miller et al., 2014; Yu et al., 2006). A common feature of epilepsy mouse models, including the *Scn1a*$^{+/-}$ Dravet model, is strain-dependent differences in phenotype severity (Bergren et al., 2005; Miller et al., 2014; Ogiwara et al., 2007; Yu et al., 2006). When the *Scn1a*$^{+/-}$ mutation is maintained on the 129S6/SvEvTac strain (129.*Scn1a*$^{+/-}$), mice display no overt seizure or neurological phenotype and experience a normal life expectancy (Miller et al., 2014). In contrast, when 129.*Scn1a*$^{+/-}$ mice are crossed to the C57BL/6 J (B6) strain, the resulting [129S6 X B6] F1.*Scn1a*$^{+/-}$ (F1.*Scn1a*$^{+/-}$) mice exhibit spontaneous generalized tonic-clonic seizures beginning at P16–19 and 75% lethality by 8 weeks of age (Miller et al., 2014). Strain differences were also observable at the level of hippocampal neurons. Hippocampal inhibitory neurons isolated from F1.*Scn1a*$^{+/-}$ mice had reduced sodium current density relative to wild-type (WT), while inhibitory neurons isolated from 129.*Scn1a*$^{+/-}$ mice were indistinguishable from WT (Mistry et al., 2014). Hippocampal pyramidal neurons from both exhibited elevated sodium current density, but the magnitude of the difference was greater

* Corresponding author at: Department of Pharmacology, Searle 8-510, 320 East Superior St, Chicago, IL 60091, USA.
E-mail address: jennifer.kearney@northwestern.edu (J.A. Kearney).

https://doi.org/10.1016/j.expneurol.2018.10.010
Received 3 April 2018; Received in revised form 11 September 2018; Accepted 18 October 2018
Available online 19 October 2018
0014-4886/

in F1.*Scn1a*$^{+/-}$ than 129.*Scn1a*$^{+/-}$ (Mistry et al., 2014). These observations suggested the B6 strain contributed modifier alleles that influence penetrance and severity of the *Scn1a*$^{+/-}$ Dravet phenotype. Using QTL mapping, we identified multiple modifier loci (*Dsm1–5*, Dravet syndrome modifier) which influence strain-dependent survival of *Scn1a*$^{+/-}$ mice (Miller et al., 2014). One locus of interest, *Dsm1*, was fine-mapped and *Gabra2* was identified as a putative modifier gene by comparing C57BL/6 J and 129S6/SvEvTac gene expression in forebrain by RNA-seq (Hawkins et al., 2016).

RNA-seq analysis has been a useful tool for identifying epilepsy modifier genes following positional cloning in various epilepsy mouse models, (Calhoun et al., 2016, 2017; Hawkins and Kearney, 2012, 2016; Hawkins et al., 2016; Thompson et al., 2017). However, the mapped modifier loci do not account for the full range of phenotypic variance. Therefore, in this study we globally characterized hippocampal gene expression in *Scn1a*$^{+/-}$ and WT mice on both the [129S6 X B6]F1 susceptible and 129S6 resistant strains at postnatal day (P) 14 and P24, during the critical time window of disease onset. The P24 F1.*Scn1a*$^{+/-}$ cohort was further subdivided into mice with and without spontaneous seizures in the 24 h prior to collection. In the absence of seizures, more genes were differentially expressed between the two strains and ages of mice rather than between *Scn1a* genotypes. As anticipated, RNA-seq analysis identified numerous changes in gene expression following seizures in the P24 F1.*Scn1a*$^{+/-}$ cohort with seizures within 24-h of sample collection.

2. Materials and methods

2.1. Mice

Scn1a^{tm1Kea} mice were generated by homologous recombination in TL1 ES cells (129S6/SvEvTac) and is maintained as a co-isogenic strain (129.*Scn1a*$^{+/-}$) by continuous backcrossing to 129S6/SvEvTac (129) (Taconic Biosciences, Hudson, NY, USA). Strain C57BL/6 J (B6) (000664, Jackson Laboratory, Bar Harbor, ME, USA) was crossed with 129.*Scn1a*$^{+/-}$ mice to generate [129 x B6]F1.*Scn1a*$^{+/-}$ mice (F1.*Scn1a*$^{+/-}$) and [129 x B6]F1.WT littermate controls (F1.WT). Mice were maintained in a Specific Pathogen Free (SPF) barrier facility with a 14-h light/10-h dark cycle and access to food and water *ad libitum*. Mice were genotyped by PCR as previously described (Miller et al., 2014). All animal care and experimental procedures were approved by the Northwestern University Animal Care and Use Committees in accordance with the National Institutes of Health Guide for the Care and Use of Laboratory Animals.

2.2. Seizure monitoring

Prior to euthanasia on P24, F1.*Scn1a*$^{+/-}$ mice were monitored for spontaneous generalized tonic-clonic seizures (GTCS) by continuous video-monitoring as previously described (Anderson et al., 2017; Hawkins et al., 2017; Hawkins et al., 2016). Briefly, mice were placed in a recording chamber (28 × 28 × 36 cm) and overhead video was captured using a Day/Night camera equipped with an infrared lens. During recording, mice had *ad libitum* access to food and water, and were maintained on a 14:10 light-dark cycle. Digital video images captured during the video-monitoring session were analyzed offline for the occurrence of spontaneous GTCS prior to pooling of tissue for RNA isolation. Previous video-EEG monitoring of F1.*Scn1a*$^{+/-}$ mice showed a perfect correlation between behavioral and electroencephalographic seizures ($\kappa = 1.0$), supporting non-invasive video monitoring as a reliable assay for GTCS detection (Hawkins et al., 2017; Hawkins et al., 2016).

2.3. RNA sample preparation

Hippocampi were dissected from 129 and F1 WT and *Scn1a*$^{+/-}$ mice at P14 and P24. Primary pools for all groups without seizures were created by combining tissue from both males ($n = 2$) and females (n = 2). For the P24 seizure cohort, primary pools were created by combining tissue from 3 or 4 mice (at least one from each sex) with seizure counts ranging from 3 to 7 in the 24 h prior to collection. Mice that had one or two GTCS prior to collection were excluded from the study. Total RNA was isolated using TRIzol reagent according to the manufacturer's instructions (Life Technologies). Following RNA isolation, RNA integrity was assessed and all samples had a RIN of ≥7.7. For each group without seizures, 2–3 superpooled biological replicates were generated by combining total RNAs from 3 to 4 primary pools ($n = 12–16$ mice/superpool) (Fig.1A). For the P24 seizure cohort, the primary pools were used as biological replicates ($n = 3–4$ mice/sample). RNA integrity was measured on the superpool samples and all samples had RIN of ≥8.1.

2.4. RNA-Seq

Samples were processed for RNA-Seq using the TruSeq RNA Library Preparation Kit v2 (Illumina, San Diego, CA, USA). Samples were sequenced on an Illumina HiSeq 4000 at BGI (Hong Kong, China). Three multiplexed lanes of 50-bp single-end sequencing resulted in almost 167 million mapped reads. Base calling and filtering of sequence reads were performed with the Illumina pipeline (Bentley et al., 2008). Bioinformatic analysis was performed on the GALAXY platform (Afgan et al., 2010; Blankenberg et al., 2010; Giardine et al., 2005). FastQ files were groomed using FastQ groomer (v. 1.0.4) aligned to the mm10 mouse genome with *Tophat2* (v. 2.1.0) (Kim et al., 2013). Counts were calculated with HTSeq (union overlap mode; v. 0.6.1p1) and differential expression was assessed with DESeq2 (v. 2.11.38) (Love et al., 2014). Differentially expressed genes were clustered based on $\log_2$(normalized expression) and heatmaps were generated using gplots for R. Gene sets were evaluated for intersections using Venny (v. 2.1.0) (Oliveros, 2007-2015), mammalian phenotype (MP) ontology, gene ontology (GO) and pathway enrichment using MouseMine (hypergeometric distribution with Holm-Bonferroni correction) and functional and protein-protein interaction enrichment using STRING (v. 10.5) (FDR adjusted *P*-values) (Motenko et al., 2015; Szklarczyk et al., 2017).

RNA-seq data discussed in this publication have been deposited in NCBI's Gene Expression Omnibus (Edgar et al., 2002) and are accessible through GEO Series accession number GSE112627 (https://www.ncbi.nlm.nih.gov/geo/query/acc.cgi?acc=GSE112627).

3. ddRT-PCR

First-strand cDNA was synthesized from 2 micrograms of total RNA using oligo(dT) primer and Superscript IV reverse transcriptase according to the manufacturer's instructions (Life Techologies). First-strand cDNA samples were diluted to be within the linear range for each assay based on empirical determination with serial dilution. Quantitative droplet digital PCR (ddPCR) was performed using ddPCR Supermix for Probes (No dUTP) (Bio-Rad, Hercules, CA, USA) and TaqMan Assays as previously described (Hawkins and Kearney, 2016). Taqman gene expression assays (Life Technologies) were: mouse Blnk (FAM-MGB-Mm01197846_m1); Gal (FAM-MGB-Mm00439056_m1); Cdk18 (FAM-MGB-Mm00432448_m1); Aspg (FAM-MGB-Mm01339695_m1); Gldn (FAM-MGB-Mm00616548_m1); Serpine1 (FAM-MGB-Mm00435858_m1); Timp1 (FAM-MGB-Mm01341361_m1); Prss23 (FAM-MGB-Mm01972869_s1); Vim (FAM-MGB–Mm013333430_m1); Gfap (VIC-MGB-Mm01253033_m1); Tbp (VIC-MGB-Mm00446971_m1); Gapdh (VIC-MGB-Mm99999915_g1).

Relative transcript levels were expressed as a concentration ratio of the gene of interest to Tbp (*Aspg, Blnk, Cdkn1a, Gal, Gldn, Prss23, Serpine1, Timp1*) or Gapdh (*Gfap, Vim*).

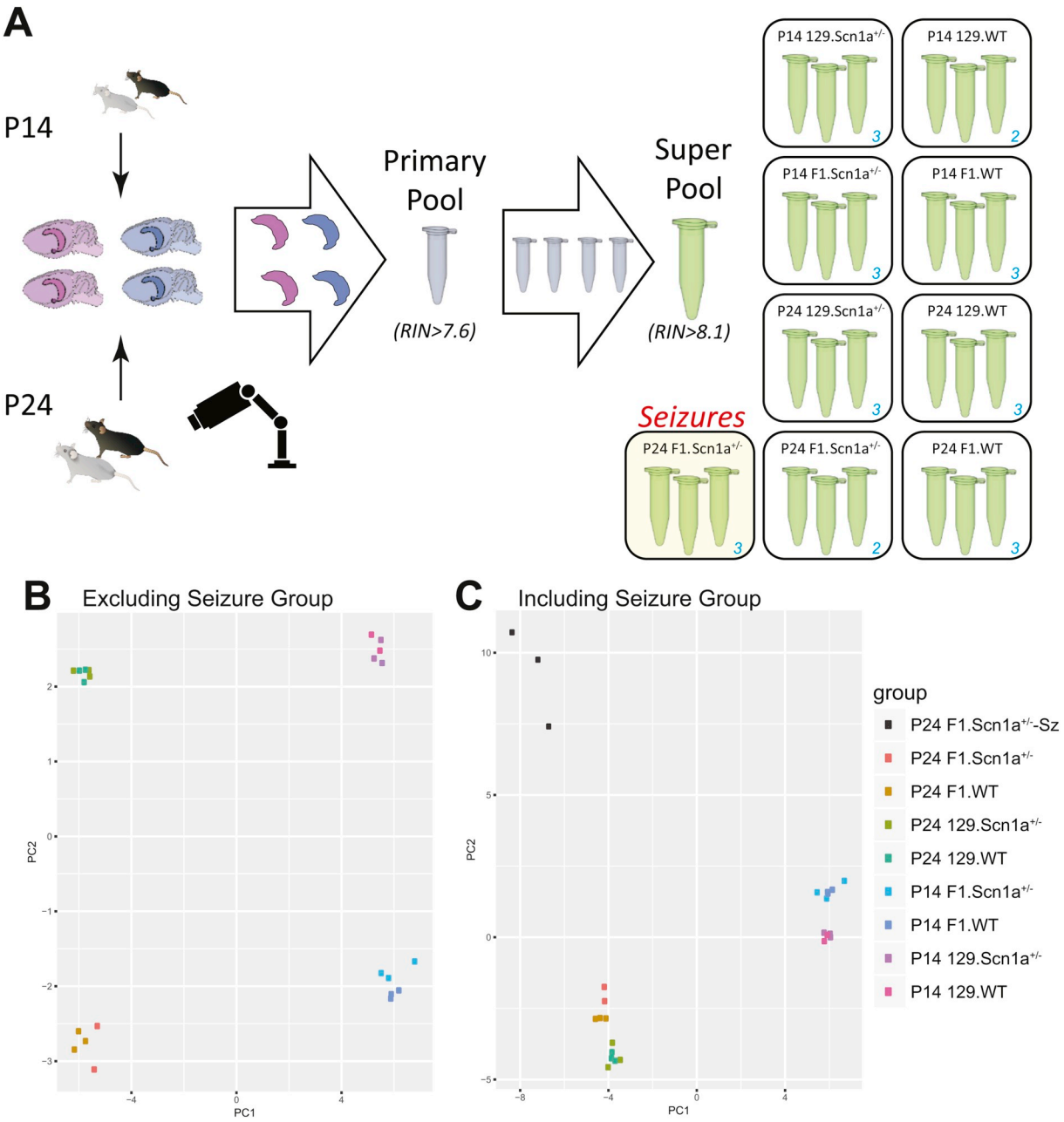

Fig. 1. Isolation and RNA-seq profiling of wild-type (WT) and *Scn1a*$^{+/-}$ mice on 129 and F1 strains at P14 and P24. A) Schematic showing collection and pooling of samples comprising the nine experimental groups. Dissected hippocampi from 4 animals (2 male, 2 female) were pooled prior to RNA isolation. Following RNA isolation, 3–4 samples with RIN > 7.6 were combined to generate superpools (n = 12–16 mice/superpool). For RNA-seq analysis 2–3 superpool biological replicates were used for each group. The number of replicates is shown in the lower left corner of the box representing the experimental groups. P24 F1.*Scn1a*$^{+/-}$ samples were further subdivided into two groups: without seizures (no shading), or with ≥3 seizures (yellow shading) within 24 h of sample collection. B&C) Sample-to-sample distances visualized by principal component analysis for experimental groups with exclusion (B) or inclusion (C) of F1.*Scn1a*$^{+/-}$ mice with seizures. (For interpretation of the references to colour in this figure legend, the reader is referred to the web version of this article.)

3.1. Immunoblotting

Hippocampal protein was isolated from P24 mice following seizure monitoring as described above. Proteins (50 µg per lane) were separated on a 7.5% SDS-PAGE gel and transferred to nitrocellulose membranes. Immunoblots were probed for GFAP using a rabbit polyclonal antibody (1:500; G9269, Sigma Aldrich) and for Mortalin using a mouse monoclonal antibody (1:1000; NeuroMab, clone 75–127). Alexa-conjugated fluorescent anti-rabbit 790 and anti-mouse 680 secondary antibodies (Jackson ImmunoResearch; 1:20,000) were used to detect bound primary antibody using an Odyssey imaging system (Licor). Relative protein levels were determined by densitometry using ImageStudio software (Licor) and expressed as a ratio of GFAP to anti-mortalin, with n = 3 biological replicates.

4. cFos immunhistochemistry

F1.*Scn1a*$^{+/-}$ mice were continuously video monitored from P21-P25 as described above. Video was rapidly reviewed multiple times per day to identify seizures and schedule perfusions post-seizure. Control tissue was obtained from F1.*Scn1a*$^{+/-}$ littermates confirmed on video to have not experienced a seizure in a minimum of 4–7 h preceding

perfusion. Mice were deeply anesthetized with Euthasol (100 mg/kg, intraperitoneal) and transcardially perfused with 0.1 M phosphate buffer followed by 4% paraformaldehyde in 0.1 M phosphate buffer. Brains were removed and postfixed overnight, cryoprotected in 30% sucrose and sectioned at 40 µm. Free-floating coronal sections were processed for cFos immunoreactivity with primary rabbit anti-c-Fos antibody (Cell Signaling Technology #2250; 1:3000). Signal was visualized using a VECTASTAIN Elite ABC HRP Kit (Vector Labs; PK-6101) and. Signal was detected using 3,3′-Diaminobenzidine tetrahydrochloride with $CoCl_2$ enhancement (Sigma-Aldrich # D0426). Sections were imaged on a TissueGnostics imaging platform with a 20× objective with automated image stitching.

5. Results

On the 129S6/SvEvTac (129) strain background, *Scn1a*$^{+/-}$ mice (129.*Scn1a*$^{+/-}$) are protected from effects of the gene deletion and have no overt phenotype, while the epilepsy phenotype is unmasked on the [129 x C57BL/6 J]F1 strain background (Miller et al., 2014). The phenotype of F1.*Scn1a*$^{+/-}$ manifests during the third postnatal week, with GTCS onset occurring at P16–19 (Miller et al., 2014). In order to characterize the hippocampal gene expression landscape, we assessed differentially expressed genes (DEGs) between genotypes (*Scn1a*$^{+/-}$ v. WT), strains (129 v. F1) and ages (P14 v. P24), as well as in the absence or presence of recent seizures at P24 (Fig. 1A; Supplementary Table 1). Overall, principal component analysis and hierarchical clustering indicated that strain and age had a more profound effect on variance than genotype in the absence of recent seizures, while inclusion of the seizure-positive group (≥3 seizures within 24-h) had a strong effect on variance (Fig. 1B-C).

5.1. Genotype-specific gene expression differences

At P14 before symptom onset, there were no hippocampal DEGs between 129.WT and 129.*Scn1a*$^{+/-}$ mice and only 21 DEGs with modest differences between F1.WT and F1.*Scn1a*$^{+/-}$ mice (Supplementary Table 2). Although the modest differences were only 6–12%-fold change, they are enriched in MP and GO terms relevant to the phenotype, including “seizures” [MP:0002064] and ‘ion transport’ and ‘ion homeostasis’ pathways (Fig. 2A-B). A similar pattern is observed at P24 with limited differences between genotypes. Only a single DEG, *Scn1a*, was identified between 129.WT and 129.*Scn1a*$^{+/-}$ mice on the protective 129 strain. On the F1 strain, P24 F1.WT and F1.*Scn1a*$^{+/-}$ mice without recent seizures had 80 DEGs with 1.12 to 1.36-fold differences (Fig. 2A; Supplementary Table 2). Again, although the differences are modest, they are enriched in MP and GO terms relevant to the phenotype (Fig. 2C; Supplementary Table 2). The observed gene expression differences between genotypes in F1 mice at P14 and P24 did not share any overlap.

5.2. Strain-specific gene expression differences

At P14, the number of hippocampal DEGs with a ≥ 1.5-fold change between 129 and F1 strains is similar in WT and *Scn1a*$^{+/-}$ mice, with 17 and 16 genes, respectively (Fig. 3A-B; Supplementary Table 3). At P24, WT mice had 41 DEGs with ≥1.5-fold difference in hippocampal expression between the 129 and F1 strains, while *Scn1a*$^{+/-}$ mice without recent seizures had ≥1.5-fold differences in 25 genes (Fig. 3A-B; Supplementary Table 3). At both ages, strain DEGs included 12 shared differences in genes encoding mainly ribosomal proteins with enrichment for protein-protein interactions (STRING PPI enrichment $p = 0.00211$) (Fig. 3B-C).

5.3. Age-specific gene expression differences

Next we compared developmental gene expression differences between P14 and P24 within the same strain and genotype in the absence of recent seizures. As expected, there were a significant number of ≥2-fold DEGs between ages for all groups, including a core set of 64 shared genes enriched for the GO term ‘nervous system development’ [GO:0007399; $p = 0.01126$] (Fig. 4A-B; Supplementary Table 4). F1.WT had the largest unique set of P14-P24 DEGs that were enriched for the GO terms ‘cell cycle’ [GO:0007049; $p = 0.036725$] and ‘cell cycle process’[GO:0022402; $p = 0.039045$] and for protein-protein interactions (STRING PPI enrichment $p < 1.0e^{-16}$) (Fig. 4B-C; Supplementary Table 4).

5.4. Seizure related gene expression differences

Seizure onset in F1.*Scn1a*$^{+/-}$ mice occurs between P16–19 (Hawkins et al., 2017; Miller et al., 2014). For this study, 64 F1.*Scn1a*$^{+/-}$ mice (32 male and 32 female) were monitored for spontaneous GTCS over a 24 h period prior to tissue collection at P24. Approximately 70% (45 F1.*Scn1a*$^{+/-}$ mice) did not experience a GTCS during the 24-h monitoring period. We previously identified the same low seizure frequency in another study (Hawkins et al., 2017). The remaining 19 F1.*Scn1a*$^{+/-}$ mice had GTCS frequencies ranging from 1 to 7 in the 24-h session. We used the seizure monitoring data to subdivide the P24 F1.*Scn1a*$^{+/-}$ cohort and compared those with and without seizures at P23–24. This allowed us to differentiate DEGs induced by acute seizure activity from those that might underlie differences in phenotype expressivity.

F1.*Scn1a*$^{+/-}$ mice having between 3 and 7 seizures within 24 h of collection on P24 were assessed for gene expression changes relative to F1.*Scn1a*$^{+/-}$ mice without seizures, as well as P24 F1.WT and 129.*Scn1a*$^{+/-}$ mice. There were numerous ≥2-fold differences in gene expression in F1.*Scn1a*$^{+/-}$ mice with seizures relative to F1.*Scn1a*$^{+/-}$ without seizures (113 DEGs), F1.WT mice (198 DEGs) and 129.*Scn1a*$^{+/-}$ mice (275 DEGs) (Fig. 5) (Supplementary Table 5). Of those, 100 were shared differences that we defined as a core set of seizure-induced DEGs (Fig. 5A; Supplementary Table 5). We compared this core set of seizure-induced DEGs with a recent set of published DEGs in another genetic epilepsy mouse model, *Scn8a*$^{N1768D/+}$, with and without seizures, as well as with rodent induced-seizure models compiled from the literature (Dingledine et al., 2017; Sprissler et al., 2017). Differential expression of 26 genes was observed in at least two of three DEG sets, and 10 DEGs were shared across all three sets (*Aspg, Blnk, Cdkn1a, Gal, Gfap, Gldn, Prss23, Serpine1, Timp1, Vim*) (Fig.5B). RNA-seq results for the core set of seizure-induced DEGs was confirmed by RT-ddPCR (Supplemental Figs. S1, S2A). The ten shared DEGs are enriched for the oxidative stress-related KEGG pathway of ‘HIF-1 signaling’ [04066; $p = 0.0034$]. A large proportion of DEGs ($n = 82$), were unique to the *Scn1a*$^{+/-}$ model and were enriched for the ontology terms: ‘cell differentiation’ [GO:0030154; $p = 0.005188$]; ‘cellular developmental process’ [GO:0048869; $p = 0.019401$]; and ‘increased anxiety-related response’ [MP:0001363; $p = 0.011173$] (Supplementary Table 5). These differences may reflect the juvenile age of onset of seizures in *Scn1a*$^{+/-}$ mice versus adult-onset of spontaneous seizures in *Scn8a*$^{N1768D/+}$ mice and adult age at the time of stimulation in induced-seizure models.

Next, we compared developmental changes from P14 to P24 between F1.*Scn1a*$^{+/-}$ mice with and without seizures. To accomplish this, we examined the intersection of the P14-P24 development gene sets, as well as DEGs between P24 F1.*Scn1a*$^{+/-}$ with and without seizures to distinguish developmental versus seizure-induced changes (Fig. 5A). Discounting seizure-induced changes, among P14-P24 DEGs for F1.*Scn1a*$^{+/-}$ mice with or without seizures, we found 68 shared DEGs versus 163 unique DEGs for F1.*Scn1a*$^{+/-}$ mice with seizures and 49 unique DEGs for F1.*Scn1a*$^{+/-}$ mice without seizures (Fig. 5C; Supplementary Table 5). Not surprisingly, shared DEGs were enriched for the GO term of ‘nervous system development’ [GO:007399; $p = 0.0134$], ‘cell development’ [GO:0048468; $p = 0.0389$] and ‘system development’ [GO:0048731; $p = 0.0389$]. The 163 DEGs

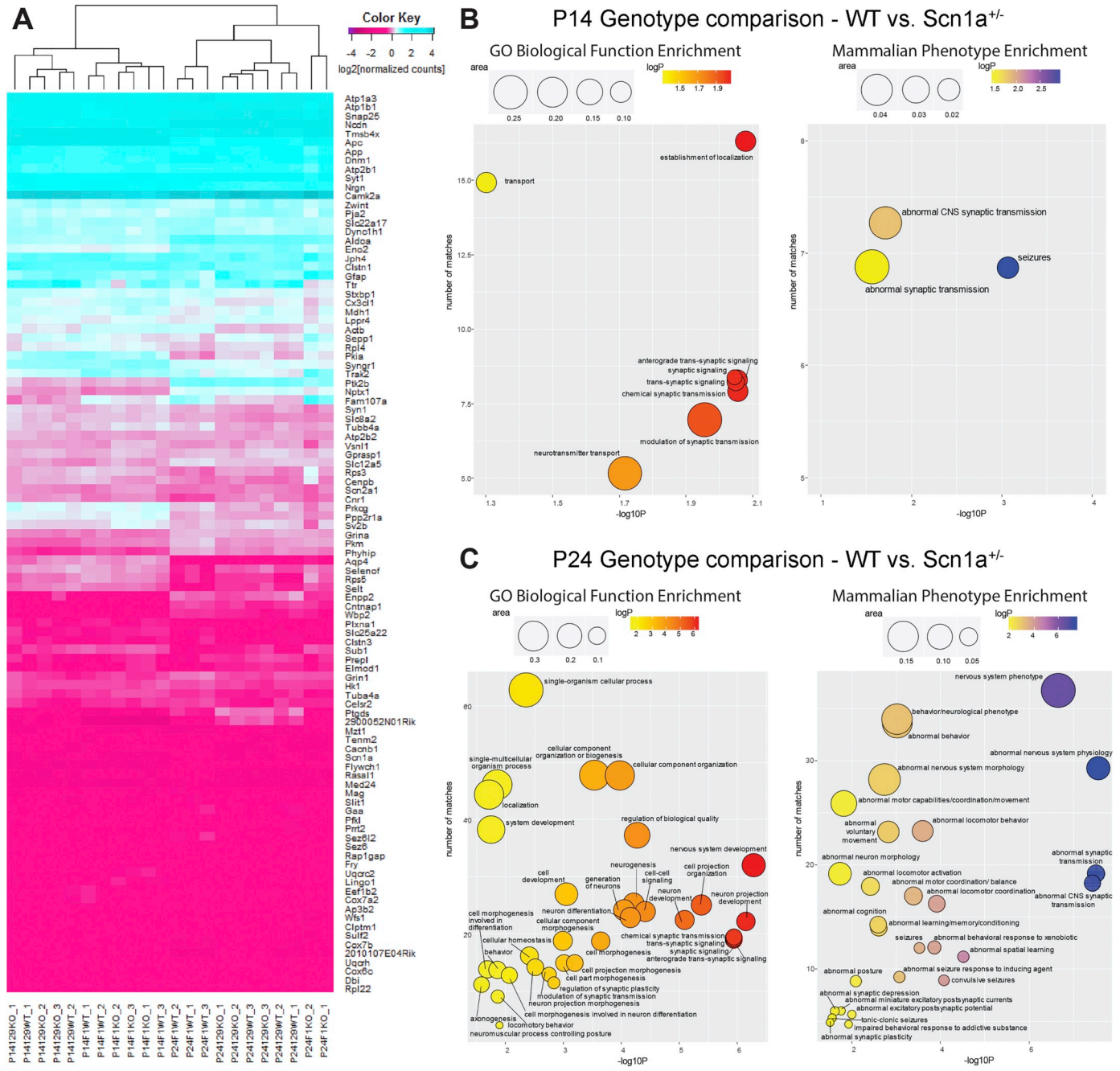

Fig. 2. Genotype-specific gene expression differences. A) Heatmap of 101 DEGs between *Scn1a*$^{+/-}$ (KO) and WT genotypes. B&C) P14 Enrichment of biological process Gene Ontology (GO) (left panel) and Mammalian phenotype (MP) ontology (right panel) at P14 (B) and P24 (C). Bubble scatterplots show the number of term matches on the y-axis and the enrichment $-\log_{10}(P)$ value on the x-axis. Bubble colour represents scaled $-\log_{10}(P)$ and area indicates frequency of the term in the underlying database. (For interpretation of the references to colour in this figure legend, the reader is referred to the web version of this article.)

unique to F1.*Scn1a*$^{+/-}$ mice with seizures were enriched for signaling/plasticity related KEGG pathways, including 'calcium signaling pathway' [04020; $p = 0.0368$] and 'neuroactive ligand-receptor interaction' [04080; p = 0.0368], as well as protein-protein interactions ($p = 8.88e^{-16}$) (Fig. 5D). The central node of this protein-protein interaction pathway is the immediate early gene Fos, which is strongly activated in the hippocampus at 1–3 h following a spontaneous seizure in *Scn1a*$^{+/-}$ mice (Fig. 5E).

6. Discussion

We previously reported strain-dependent differences in phenotype expressivity in the *Scn1a*$^{+/-}$ Dravet model (Miller et al., 2014). In the current study we profiled global hippocampal gene expression across different genotypes, strains and ages to assess potential transcriptional differences that may underlie the observed strain-dependence of the *Scn1a*$^{+/-}$ Dravet model. This analysis included examining gene expression differences by genotype, strain, age, and seizure status. Overall, the magnitude of gene expression differences between genotypes was modest, between strains was moderate, and between age or seizure status were largest. The specific comparisons and their potential implications are discussed in more detail below.

6.1. Genotype-specific gene expression differences

Remarkably, there were no differences in gene expression between

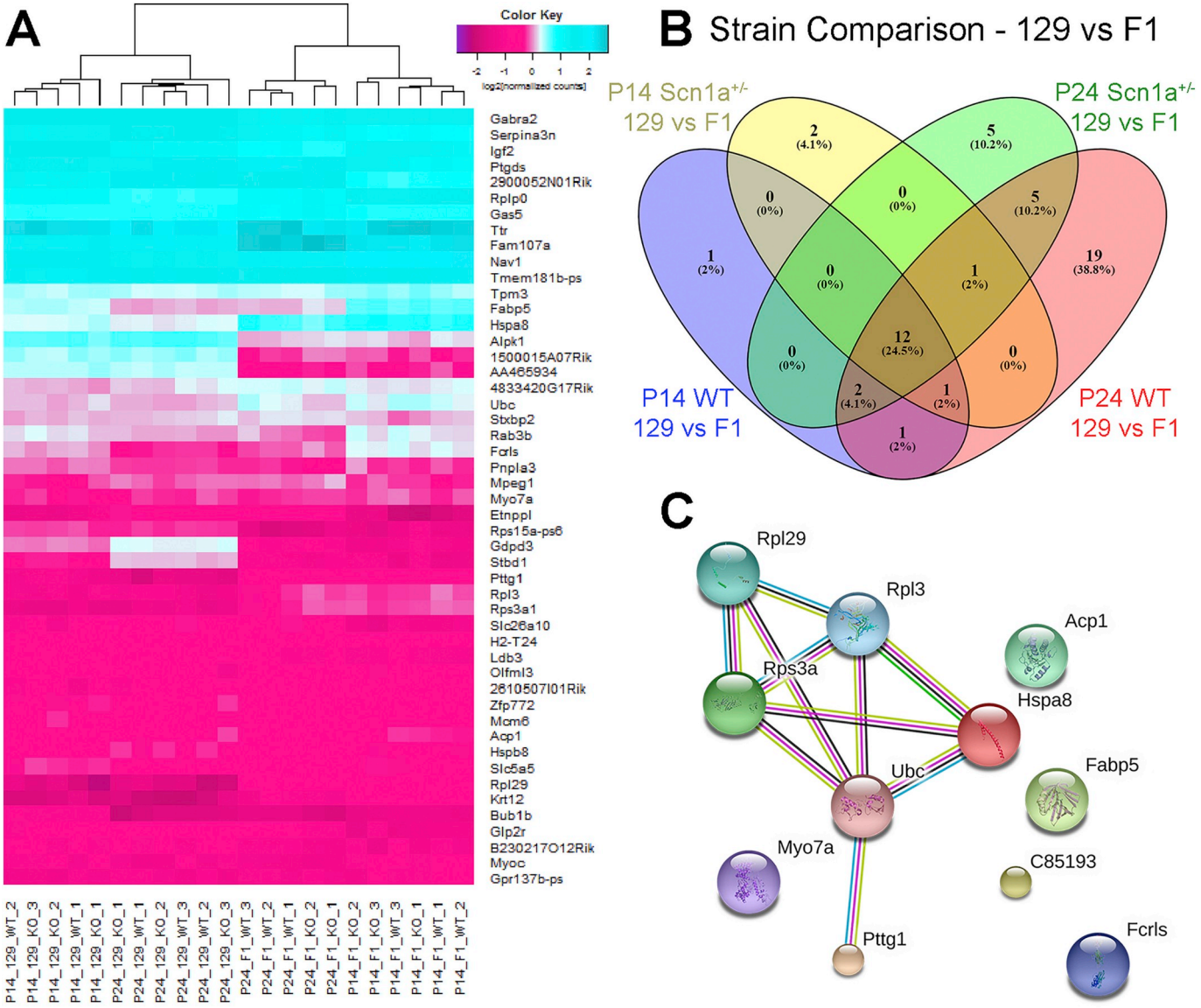

Fig. 3. Strain-specific gene expression differences. A) Heatmap of 99 DEGs between 129 and F1 strains. B) Four way venn diagram of strain-specific DEGs. C) Protein-protein interaction network of shared set of 12 strain-specific DEGs (STRING database v. 10.5).

129.WT and 129.*Scn1a*$^{+/-}$ mice at P14 or P24, aside from an expected decrement in *Scn1a* transcript in 129.*Scn1a*$^{+/-}$ mice. This suggests that the protective 129 strain background may be buffered against transcriptional changes in the context of heterozygous deletion of *Scn1a*. In contrast, on the susceptible F1 strain, there were modest differences in gene expression at P14 and P24. Although the differences were small, ranging from 6 to 12%-fold change at P14 and 12–36%-fold change at P24, gene set enrichment analysis demonstrated enrichment in GO and MP terms relevant to the phenotype, including synaptic signaling, neurodevelopment, abnormal nervous system physiology and seizure-related terms, among others. This accumulation of modest changes in a collection of relevant genes may potentially reflect homeostatic plasticity mechanisms that attempt to rebalance neuronal excitability in response to *Scn1a*$^{+/-}$ deletion in the F1 strain. It is also possible that the limited number and small magnitude of genotype-specific differences may result from dampening of signals from minor cells types within the bulk hippocampal tissue. Future gene expression studies of isolated hippocampal cell types will investigate this possibility.

Interestingly, the only observed change in expression of other voltage-gated sodium channel genes was a modest 11% difference in *Scn2a* expression between P14 F1.*Scn1a*$^{+/-}$ and F1.WT mice. Previous reports of *Scn8a*^{medtg} and *Scn8a*^{medJ} null and hypomorphic alleles have demonstrated compensatory actions of Nav1.1 and Nav1.2 at the protein level, but there is no evidence of corresponding transcriptional upregulation of *Scn1a* and *Scn2a* (Kearney et al., 2002; Van Wart and Matthews, 2006; Vega et al., 2008).

6.2. Strain-specific gene expression differences

There were a total 49 genes with ≥1.5-fold differential expression between 129 and F1 strains. Notable among these was *Gabra2*, which we previously identified as a genetic modifier that influences the *Scn1a*$^{+/-}$ survival phenotype (Hawkins et al., 2016). Strain-specific DEGs included 12 differences shared across both ages and genotypes (Fig. 3B). These shared differences were enriched for genes encoding ribosomal proteins (Fig. 3C). Differential and dynamic expression of ribosomal protein has been previously reported across developmental stages, raising the possibility that F1 and 129 mice may differ in hippocampal developmental trajectory between P14 and P24 (Kondrashov et al., 2011; Kraushar et al., 2016; Perucho et al., 2014).

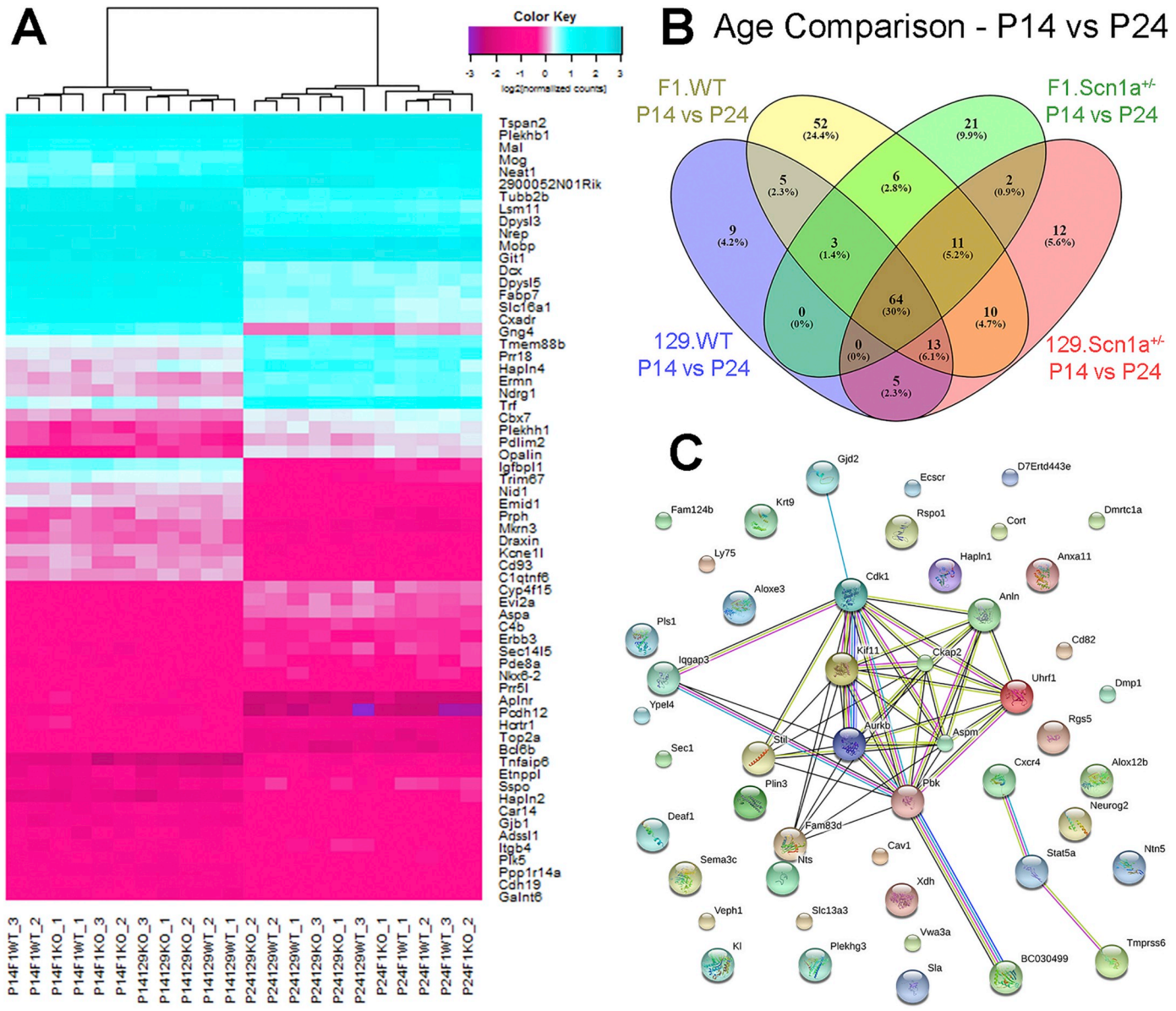

Fig. 4. Age-specific gene expression differences. A) Heatmap of DEGs between P14 and P24 mice. B) Four way venn diagram of age-specific DEGs. C) Protein-protein interaction network of 52 developmental DEGs unique to F1.WT mice (STRING database v. 10.5).

6.3. Age-specific gene expression differences

We observed a significant number of ≥2-fold DEGs between P14 and P24, as expected, including a shared set of 64 core genes enriched for the GO term 'nervous system development'. While 129.*Scn1a*$^{+/-}$ and 129.WT had relatively few unique DEGs between P14 and P24, F1.WT and F1.*Scn1a*$^{+/-}$ had 52 and 21 unique DEGs, respectively. Although there was no significant term enrichment in the F1.*Scn1a*$^{+/-}$ group, F1.WT DEGs were enriched for the GO terms 'cell cycle' and 'cell cycle process' and for protein-protein interactions. The pattern of DEG enrichment suggests upregulation of mitotic activity and neurogenesis in the F1.WT mice from P14 to P24. This again raises the possibility that F1.WT and 129.WT mice may differ in hippocampal developmental trajectory in the third week of life.

6.4. Seizure related gene expression differences

As expected, spontaneous seizure activity induced many changes in gene expression. We observed 113 ≥ 2-fold DEGs between P24 F1.*Scn1a*$^{+/-}$ mice with and without seizures in the antecedent 24 h. Further comparison with F1.WT mice and 129.*Scn1a*$^{+/-}$ mice allowed us to define a core set of 100 seizure-induced DEGs. Comparison of our core set of seizure-induced DEGs with DEG sets from another genetic epilepsy model, *Scn8a*$^{N1768D/+}$ and rodent-induced seizure models, identified a set of 10 DEGs that were shared among these models. Although there was only a 10% overlap of specific DEGs, there are numerous differences between the models, including age of seizure onset, strain background and species (mouse vs. rat), as well as RNA preparation, evaluation and analysis platforms. Thus, these 10 DEGs represent the most robust seizure-induced changes and may serve as broad candidates for neuroprotection. Half of the shared DEGs are associated with astrogliosis (Zamanian et al., 2012; Zhang et al., 2016), and consistent with this we observed a trend toward increase GFAP protein in the hippocampus of F1.*Scn1a*$^{+/-}$ mice with seizures relative to those without seizures in the antecedent 24 h (Fig. S2). Overall, this robust set of shared DEGs includes genes known to be elevated in response to seizures or traumatic brain injury in human and rodent models (Almeida-Suhett et al., 2014; Dingledine et al., 2017; Johnson

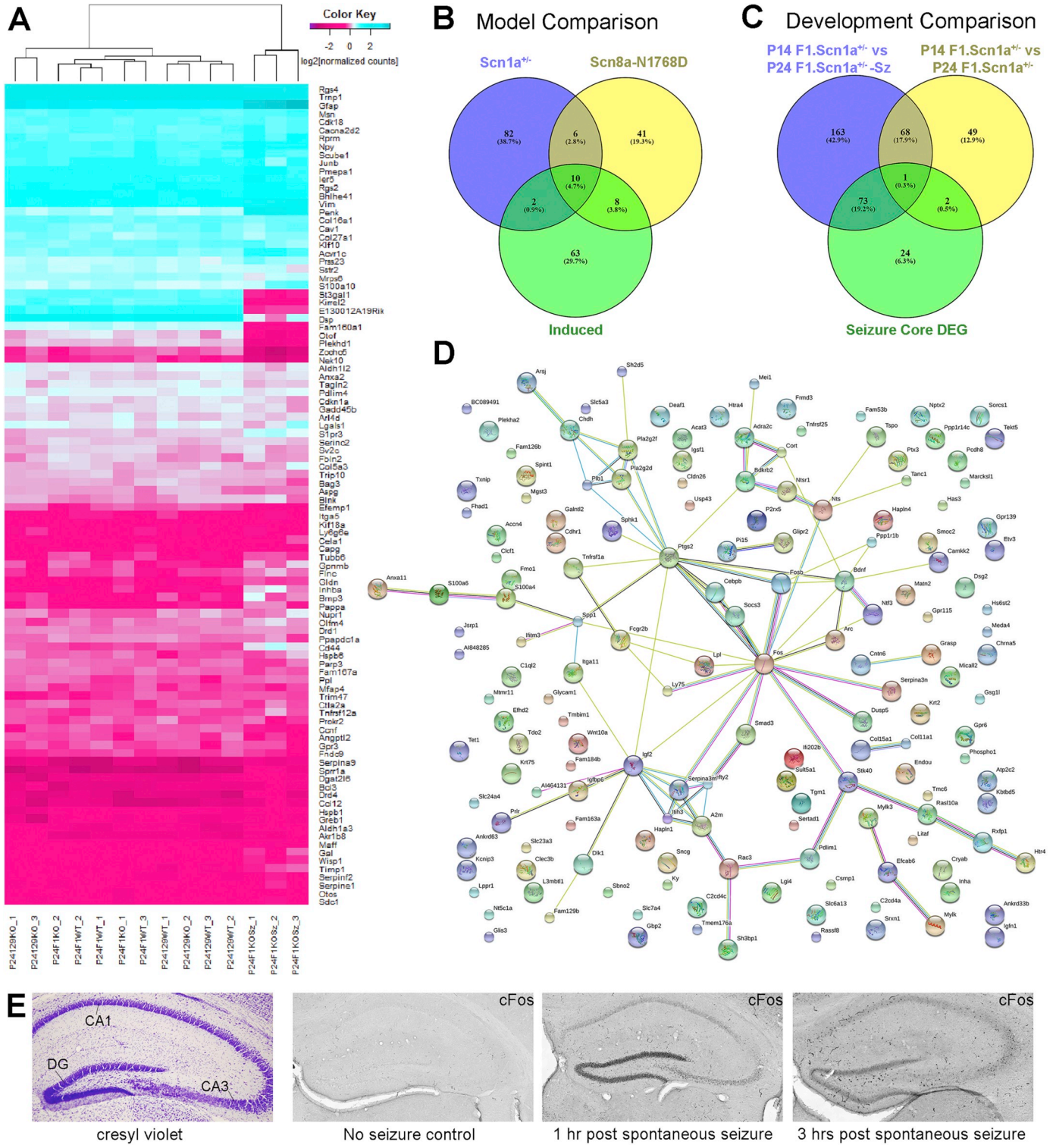

Fig. 5. Seizure-related gene expression differences. A) Heatmap of 100 core DEGs induced by acute seizure activity ≤24 h prior to sample collection. B) Venn diagram showing overlap between seizure-related DEGs in F1.*Scn1a*$^{+/-}$ mice, *Scn8a*$^{N1768D/+}$ mice and induced-seizure models (Dingledine et al., 2017; Sprissler et al., 2017). C) Venn diagram showing overlap of developmental changes between F1.*Scn1a*$^{+/-}$ mice with seizures (Sz)(blue) and without seizures (yellow), along with DEGs between P24 seizure and no-seizure groups (green). D) Protein-protein interaction network of 163 developmental DEGs unique to F1.*Scn1a*$^{+/-}$ mice with seizures (STRING database v. 10.5). E) Representative images for hippocampal c-Fos immunoreactivity are shown for F1.*Scn1a*$^{+/-}$ mice post-spontaneous seizure, and F1.*Scn1a*$^{+/-}$ mice with no seizure. The left panel is a cresyl violet stained hippocampal section for orientation. (For interpretation of the references to colour in this figure legend, the reader is referred to the web version of this article.)

et al., 2015; Samal et al., 2015; Sprissler et al., 2017). This suggests that these changes are a consequence of the insult rather than a cause, but it is not possible to parse whether these expression alterations are adaptive or maladaptive based on gene expression studies alone.

We also compared developmental changes from P14 to P24 between F1.*Scn1a*$^{+/-}$ mice with and without seizures, following exclusion of

acute seizure-induced DEGs in order to separate injury induced changes from potential homeostatic changes. This analysis revealed 68 shared DEGs versus 163 unique DEGs with seizures, or 49 unique DEGs without seizures. Shared DEGs were enriched for 'nervous system development', 'cell development' and 'gliogenesis' GO terms, consistent with expectations as mouse hippocampus continues to develop between P14 and P24. Interestingly, the DEG set unique to F1.*Scn1a*$^{+/-}$ mice with seizures (excluding acute seizure-induced DEGs discussed above) was enriched for signaling/plasticity related KEGG pathways, including 'calcium signaling pathway' and 'neuroactive ligand-receptor interaction', suggesting that homeostatic plasticity occurs in the hippocampus in response to seizure activity. This is consistent with the long-standing hypothesis that homeostatic plasticity occurs in response to seizure activity and/or brain injury, and failure of these mechanisms to adequately rebalance excitability contributes to the development and progression of epilepsy.

7. Conclusion

Our previous modifier mapping studies relied on RNA-seq comparisons between WT mice of the resistant and permissive background strains. This revealed intrinsic strain differences, but did not account for differences in strain response to the primary driver mutation. Here we used gene expression profiling to characterize genome-wide differences in the context of the driver mutation which may reveal additional modifiers that contribute to the variable phenotype of *Scn1a*$^{+/-}$ mice. Furthermore, this analysis may suggest additional genes which influence seizure manifestation, independent of the previously identified Dravet survival modifier loci (Miller et al., 2014). Future studies will evaluate the contribution of unique DEGs identified between F1. *Scn1a*$^{+/-}$ mice with and without seizures that are related to acute seizure activity to determine whether they influence presentation or frequency of seizures in the *Scn1a*$^{+/-}$ Dravet mouse model.

Supplementary data to this article can be found online at https://doi.org/10.1016/j.expneurol.2018.10.010.

Acknowledgements

We thank Nicole Zachwieja for technical support. This work was support by the National Institutes of Health [R01 NS084959 (JAK)].

Declarations of interest

None.

References

Afgan, E., Baker, D., Coraor, N., Chapman, B., Nekrutenko, A., Taylor, J., 2010. Galaxy CloudMan: delivering cloud compute clusters. BMC bioinformatics 11 (Suppl. 12), S4.

Almeida-Suhett, C.P., Li, Z., Marini, A.M., Braga, M.F., Eiden, L.E., 2014. Temporal course of changes in gene expression suggests a cytokine-related mechanism for long-term hippocampal alteration after controlled cortical impact. J. Neurotrauma 31, 683–690.

Anderson, L.L., Hawkins, N.A., Thompson, C.H., Kearney, J.A., George Jr., A.L., 2017. Unexpected Efficacy of a Novel Sodium Channel Modulator in Dravet Syndrome. Sci. Rep. 7, 1682.

Bentley, D.R., Balasubramanian, S., Swerdlow, H.P., Smith, G.P., Milton, J., Brown, C.G., Hall, K.P., Evers, D.J., Barnes, C.L., Bignell, H.R., Boutell, J.M., Bryant, J., Carter, R.J., Keira Cheetham, R., Cox, A.J., Ellis, D.J., Flatbush, M.R., Gormley, N.A., Humphray, S.J., Irving, L.J., Karbelashvili, M.S., Kirk, S.M., Li, H., Liu, X., Maisinger, K.S., Murray, L.J., Obradovic, B., Ost, T., Parkinson, M.L., Pratt, M.R., Rasolonjatovo, I.M., Reed, M.T., Rigatti, R., Rodighiero, C., Ross, M.T., Sabot, A., Sankar, S.V., Scally, A., Schroth, G.P., Smith, M.E., Smith, V.P., Spiridou, A., Torrance, P.E., Tzonev, S.S., Vermaas, E.H., Walter, K., Wu, X., Zhang, L., Alam, M.D., Anastasi, C., Aniebo, I.C., Bailey, D.M., Bancarz, I.R., Banerjee, S., Barbour, S.G., Baybayan, P.A., Benoit, V.A., Benson, K.F., Bevis, C., Black, P.J., Boodhun, A., Brennan, J.S., Bridgham, J.A., Brown, R.C., Brown, A.A., Buermann, D.H., Bundu, A.A., Burrows, J.C., Carter, N.P., Castillo, N., Chiara, E.C.M., Chang, S., Neil Cooley, R., Crake, N.R., Dada, O.O., Diakoumakos, K.D., Dominguez-Fernandez, B., Earnshaw, D.J., Egbujor, U.C., Elmore, D.W., Etchin, S.S., Ewan, M.R., Fedurco, M., Fraser, L.J., Fuentes Fajardo, K.V., Scott Furey, W., George, D., Gietzen, K.J., Goddard, C.P., Golda, G.S., Granieri, P.A., Green, D.E., Gustafson, D.L., Hansen, N.F., Harnish, K., Haudenschild, C.D., Heyer, N.I., Hims, M.M., Ho, J.T., Horgan, A.M., Hoschler, K., Hurwitz, S., Ivanov, D.V., Johnson, M.Q., James, T., Huw Jones, T.A., Kang, G.D., Kerelska, T.H., Kersey, A.D., Khrebtukova, I., Kindwall, A.P., Kingsbury, Z., Kokko-Gonzales, P.I., Kumar, A., Laurent, M.A., Lawley, C.T., Lee, S.E., Lee, X., Liao, A.K., Loch, J.A., Lok, M., Luo, S., Mammen, R.M., Martin, J.W., McCauley, P.G., McNitt, P., Mehta, P., Moon, K.W., Mullens, J.W., Newington, T., Ning, Z., Ling Ng, B., Novo, S.M., O'Neill, M.J., Osborne, M.A., Osnowski, A., Ostadan, O., Paraschos, L.L., Pickering, L., Pike, A.C., Pike, A.C., Chris Pinkard, D., Pliskin, D.P., Podhasky, J., Quijano, V.J., Raczy, C., Rae, V.H., Rawlings, S.R., Chiva Rodriguez, A., Roe, P.M., Rogers, J., Rogert Bacigalupo, M.C., Romanov, N., Romieu, A., Roth, R.K., Rourke, N.J., Ruediger, S.T., Rusman, E., Sanches-Kuiper, R.M., Schenker, M.R., Seoane, J.M., Shaw, R.J., Shiver, M.K., Short, S.W., Sizto, N.L., Sluis, J.P., Smith, M.A., Ernest Sohna Sohna, J., Spence, E.J., Stevens, K., Sutton, N., Szajkowski, L., Tregidgo, C.L., Turcatti, G., Vandevondele, S., Verhovsky, Y., Virk, S.M., Wakelin, S., Walcott, G.C., Wang, J., Worsley, G.J., Yan, J., Yau, L., Zuerlein, M., Rogers, J., Mullikin, J.C., Hurles, M.E., McCooke, N.J., West, J.S., Oaks, F.L., Lundberg, P.L., Klenerman, D., Durbin, R., Smith, A.J., 2008. Accurate whole human genome sequencing using reversible terminator chemistry. Nature 456, 53–59.

Bergren, S.K., Chen, S., Galecki, A., Kearney, J.A., 2005. Genetic modifiers affecting severity of epilepsy caused by mutation of sodium channel Scn2a. Mamm. Genome 16, 683–690.

Blankenberg, D., Von Kuster, G., Coraor, N., Ananda, G., Lazarus, R., Mangan, M., Nekrutenko, A., Taylor, J., 2010. Galaxy: a web-based genome analysis tool for experimentalists. Current protocols in molecular biology Chapter 19 (Unit 19.10.11-21).

Calhoun, J.D., Hawkins, N.A., Zachwieja, N.J., Kearney, J.A., 2016. Cacna1g is a genetic modifier of epilepsy caused by mutation of voltage-gated sodium channel Scn2a. Epilepsia 57, e103–e107.

Calhoun, J.D., Hawkins, N.A., Zachwieja, N.J., Kearney, J.A., 2017. Cacna1g is a genetic modifier of epilepsy in a mouse model of Dravet syndrome. Epilepsia 58, e111–e115.

Claes, L.R.F., Deprez, L., Suls, A., Baets, J., Smets, K., Van Dyck, T., Deconinck, T., Jordanova, A., De Jonghe, P., 2009. The SCN1A variant database: a novel research and diagnostic tool. Hum. Mutat. 30, 904–920.

De Jonghe, P., 2011. Molecular genetics of Dravet syndrome. Dev. Med. Child Neurol. 53 (Suppl. 2), 7–10.

Dingledine, R., Coulter, D.A., Fritsch, B., Gorter, J.A., Lelutiu, N., McNamara, J., Nadler, J.V., Pitkanen, A., Rogawski, M.A., Skene, P., Sloviter, R.S., Wang, Y., Wadman, W.J., Wasterlain, C., Roopra, A., 2017. Transcriptional profile of hippocampal dentate granule cells in four rat epilepsy models. Scientific data 4, 170061.

Dravet, C., 2011. The core Dravet syndrome phenotype. Epilepsia 52 (Suppl. 2), 3–9.

Dravet, C., Oguni, H., 2013. Dravet syndrome (severe myoclonic epilepsy in infancy). Handb. Clin. Neurol. 111, 627–633.

Edgar, R., Domrachev, M., Lash, A.E., 2002. Gene Expression omnibus: NCBI gene expression and hybridization array data repository. Nucleic Acids Res. 30, 207–210.

Giardine, B., Riemer, C., Hardison, R.C., Burhans, R., Elnitski, L., Shah, P., Zhang, Y., Blankenberg, D., Albert, I., Taylor, J., Miller, W., Kent, W.J., Nekrutenko, A., 2005. Galaxy: a platform for interactive large-scale genome analysis. Genome Res. 15, 1451–1455.

Hawkins, N.A., Kearney, J.A., 2012. Confirmation of an epilepsy modifier locus on mouse chromosome 11 and candidate gene analysis by RNA-Seq. Genes Brain Behav. 11, 452–460.

Hawkins, N.A., Kearney, J.A., 2016. Hlf is a genetic modifier of epilepsy caused by voltage-gated sodium channel mutations. Epilepsy Res. 119, 20–23.

Hawkins, N.A., Zachwieja, N.J., Miller, A.R., Anderson, L.L., Kearney, J.A., 2016. Fine Mapping of a Dravet Syndrome Modifier Locus on Mouse Chromosome 5 and Candidate Gene Analysis by RNA-Seq. PLoS Genet. 12, e1006398.

Hawkins, N.A., Anderson, L.L., Gertler, T.S., Laux, L., George Jr., A.L., Kearney, J.A., 2017. Screening of conventional anticonvulsants in a genetic mouse model of epilepsy. Annals of clinical and translational neurology 4, 326–339.

Johnson, M.R., Behmoaras, J., Bottolo, L., Krishnan, M.L., Pernhorst, K., Santoscoy, P.L.M., Rossetti, T., Speed, D., Srivastava, P.K., Chadeau-Hyam, M., Hajji, N., Dabrowska, A., Rotival, M., Razzaghi, B., Kovac, S., Wanisch, K., Grillo, F.W., Slaviero, A., Langley, S.R., Shkura, K., Roncon, P., De, T., Mattheisen, M., Niehusmann, P., O'Brien, T.J., Petrovski, S., von Lehe, M., Hoffmann, P., Eriksson, J., Coffey, A.J., Cichon, S., Walker, M., Simonato, M., Danis, B., Mazzuferi, M., Foerch, P., Schoch, S., De Paola, V., Kaminski, R.M., Cunliffe, V.T., Becker, A.J., Petretto, E., 2015. Systems genetics identifies Sestrin 3 as a regulator of a proconvulsant gene network in human epileptic hippocampus. Nat. Commun. 6, 6031.

Kalume, F., Westenbroek, R.E., Cheah, C.S., Yu, F.H., Oakley, J.C., Scheuer, T., Catterall, W.A., 2013. Sudden unexpected death in a mouse model of Dravet syndrome. J. Clin. Invest. 123, 1798–1808.

Kearney, J.A., Buchner, D.A., De Haan, G., Adamska, M., Levin, S.I., Furay, A.R., Albin, R.L., Jones, J.M., Montal, M., Stevens, M.J., Sprunger, L.K., Meisler, M.H., 2002. Molecular and pathological effects of a modifier gene on deficiency of the sodium channel Scn8a (Na(v)16). Human molecular genetics 11, 2765–2775.

Kim, D., Pertea, G., Trapnell, C., Pimentel, H., Kelley, R., Salzberg, S.L., 2013. TopHat2: accurate alignment of transcriptomes in the presence of insertions, deletions and gene fusions. Genome Biol. 14, R36.

Kondrashov, N., Pusic, A., Stumpf, C.R., Shimizu, K., Hsieh, A.C., Ishijima, J., Shiroishi, T., Barna, M., 2011. Ribosome-mediated specificity in Hox mRNA translation and vertebrate tissue patterning. Cell 145, 383–397.

Kraushar, M.L., Popovitchenko, T., Volk, N.L., Rasin, M.-R., 2016. The frontier of RNA metamorphosis and ribosome signature in neocortical development. International journal of developmental neuroscience 55, 131–139.

Love, M.I., Huber, W., Anders, S., 2014. Moderated estimation of fold change and

dispersion for RNA-seq data with DESeq2. Genome Biol. 15, 550.
Miller, A.R., Hawkins, N.A., McCollom, C.E., Kearney, J.A., 2014. Mapping genetic modifiers of survival in a mouse model of Dravet syndrome. Genes Brain Behav. 13, 163–172.
Mistry, A.M., Thompson, C.H., Miller, A.R., Vanoye, C.G., George Jr., A.L., Kearney, J.A., 2014. Strain- and age-dependent hippocampal neuron sodium currents correlate with epilepsy severity in Dravet syndrome mice. Neurobiol. Dis. 65, 1–11.
Motenko, H., Neuhauser, S.B., O'Keefe, M., Richardson, J.E., 2015. MouseMine: a new data warehouse for MGI. Mamm. Genome 26, 325–330.
Ogiwara, I., Miyamoto, H., Morita, N., Atapour, N., Mazaki, E., Inoue, I., Takeuchi, T., Itohara, S., Yanagawa, Y., Obata, K., Furuichi, T., Hensch, T.K., Yamakawa, K., 2007. Nav1.1 localizes to axons of parvalbumin-positive inhibitory interneurons: a circuit basis for epileptic seizures in mice carrying an Scn1a gene mutation. J. Neurosci. 27, 5903–5914.
Oliveros, J.C., 2007-2015. Venny. An Interactive Tool for Comparing Lists with Venn's Diagrams.
Perucho, L., Artero-Castro, A., Guerrero, S., Ramón Y Cajal, S., Lleonart, M.E., Wang, Z.-Q., 2014. RPLP1, a crucial Ribosomal Protein for Embryonic Development of the nervous System. PLoS One 9, e99956.
Samal, B.B., Waites, C.K., Almeida-Suhett, C., Li, Z., Marini, A.M., Samal, N.R., Elkahloun, A., Braga, M.F., Eiden, L.E., 2015. Acute Response of the Hippocampal Transcriptome following Mild Traumatic Brain Injury after Controlled Cortical Impact in the Rat. Journal of molecular neuroscience 57, 282–303.
Scheffer, I.E., Zhang, Y.-H., Jansen, F.E., Dibbens, L., 2009. Dravet syndrome or genetic (generalized) epilepsy with febrile seizures plus? Brain and Development 31, 394–400.
Sprissler, R.S., Wagnon, J.L., Bunton-Stasyshyn, R.K., Meisler, M.H., Hammer, M.F., 2017. Altered gene expression profile in a mouse model of SCN8A encephalopathy. Exp. Neurol. 288, 134–141.
Szklarczyk, D., Morris, J.H., Cook, H., Kuhn, M., Wyder, S., Simonovic, M., Santos, A., Doncheva, N.T., Roth, A., Bork, P., Jensen, L.J., von Mering, C., 2017. The STRING database in 2017: quality-controlled protein-protein association networks, made broadly accessible. 45. pp. D362–d368.
Thompson, C.H., Hawkins, N.A., Kearney, J.A., George Jr., A.L., 2017. CaMKII modulates sodium current in neurons from epileptic Scn2a mutant mice. Proc. Natl. Acad. Sci. U. S. A. 114, 1696–1701.
Van Wart, A., Matthews, G., 2006. Impaired firing and cell-specific compensation in neurons lacking nav1.6 sodium channels. J. Neurosci. 26, 7172–7180.
Vega, A.V., Henry, D.L., Matthews, G., 2008. Reduced expression of Na(v)1.6 sodium channels and compensation by Na(v)1.2 channels in mice heterozygous for a null mutation in Scn8a. Neurosci. Lett. 442, 69–73.
Yu, F.H., Mantegazza, M., Westenbroek, R.E., Robbins, C.A., Kalume, F., Burton, K.A., Spain, W.J., McKnight, G.S., Scheuer, T., Catterall, W.A., 2006. Reduced sodium current in GABAergic interneurons in a mouse model of severe myoclonic epilepsy in infancy. Nat. Neurosci. 9, 1142–1149.
Zamanian, J.L., Xu, L., Foo, L.C., Nouri, N., Zhou, L., Giffard, R.G., Barres, B.A., 2012. Genomic Analysis of Reactive Astrogliosis. J. Neurosci. 32, 6391–6410.
Zhang, Y., Sloan, S.A., Clarke, L.E., Caneda, C., Plaza, C.A., Blumenthal, P.D., Vogel, H., Steinberg, G.K., Edwards, M.S., Li, G., Duncan 3rd, J.A., Cheshier, S.H., Shuer, L.M., Chang, E.F., Grant, G.A., Gephart, M.G., Barres, B.A., 2016. Purification and Characterization of Progenitor and Mature Human Astrocytes reveals Transcriptional and Functional differences with Mouse. Neuron 89, 37–53.